Real-Time Load Impedance Optimization for Radar Spectral Mask Compliance and Power Efficiency

MATTHEW FELLOWS, Student Member, IEEE
CHARLES BAYLIS, Member, IEEE
Baylor University
Waco, TX, USA

LAWRENCE COHEN, Senior Member, IEEE
Naval Research Laboratory
Washington, DC, USA

ROBERT J. MARKS II, Fellow, IEEE
Baylor University
Waco, TX, USA

This paper presents a fast optimization algorithm for power amplifiers in radar transmitters based upon a metric designed to assess spectral mask compliance. The search finds the load impedance maximizing the power-added efficiency (PAE) while providing compliance with the assigned spectral mask. Measurement results illustrate consistency in the chosen optimum values of efficiency, while spectral mask requirements are consistently met at the optimum load impedances chosen by the search. This algorithm will allow adaptive radar transmitter amplifiers to quickly adjust their load impedances to change frequency bands of operation, change spectral output properties based on nearby spectrum users, and meet dynamically varying spectral mask requirements.

Manuscript received December 19, 2013; revised April 9, 2014, September 2, 2014; released for publication September 4, 2014.

DOI. No. 10.1109/TAES.2014.130825.

Refereeing of this contribution was handled by S. Watts.

This work has been funded under a grant from the National Science Foundation (Award ECCS-1343316).

Authors' address: Department of Electrical and Computer Engineering, Baylor University, One Bear Place #97356, Waco, TX 76798-7356, USA. E-mail: (Charles_Baylis@Baylor.edu).

I. INTRODUCTION

The recent rise in demand for wireless broadband communication devices has brought increasing concern to radar operators. The growth in wireless broadband applications and users indicates that future radars will have to operate more flexibly and use less spectrum. Many believe that dynamic spectrum access (DSA), a protocol wherein spectrum is assigned in real time, will be the sharing protocol of the future and that future spectrum users will need to be flexible in transmission frequency, power, and bandwidth to meet ever-changing spectral environments. For radar operators, one potentially useful idea is cognitive radar, thoroughly discussed by Haykin [1] and Guerci [2]. A cognitive radar senses and adapts to its environment and to regulations. A significant challenge in building an adaptive radar is the creation of adaptable transmitter circuitry and corresponding algorithms that can adjust the characteristics of the circuitry for operation at different operating frequencies, as well as adjust to changing spectral mask requirements. In the future, it is possible that spectral mask requirements for the radar may change in different regions, and may be based on the number of active spectrum users in a geographical area. The circuitry must be able to reconfigure quickly to minimize the radar "down time" for adjustment.

A phased-array radar transmitter normally consists of multiple amplifiers connected to antennas. The development of microwave microelectrical mechanical system (MEMS) technology for tunable circuits, as demonstrated by Qiao et al. in [19], is a potential way that tunable passive matching networks could be constructed in future radar transmitters. The tunable MEMS circuitry would be placed following each amplifier's active device as its output matching network, allowing load impedances around the Smith chart to be accomplished and changed "on the fly" during radar operation. We present algorithms and bench-top measurement results to serve as a starting point for real-time tuning of amplifier circuitry for changing optimization objectives, as in a DSA or dynamic spectral mask environment. Parallel development in microwave MEMS technologies and reconfigurable circuitry are expected to support the implementation of tunable circuitry in future radar systems.

In this paper, we present an algorithm to optimize the transmitter's output based directly on the spectral mask. Radar transmitter output signals are required to be within the confines of a spectral mask, determined according to the standards of the International Telecommunication Union (ITU) and, in the United States, the National Telecommunications and Information Administration (NTIA) and Federal Communications Commission (FCC). ITU standard ITU-R SM.329 discusses allowable spectral emissions in the spurious emission domain [3], and standard ITU-R SM.1541 discusses allowable spectral emissions in the out-of-band domain, which is closer to the assigned bandwidth than the spurious domain [4]. The ITU Radio Regulations provide information regarding the

spectral limitation requirements of transmitted radio signals [5]. In the United States, the Radar Spectrum Engineering Criteria (RSEC) specifically describes the guidelines for radar spectrum emissions [6].

In a previous paper, we presented and demonstrated a vector-based algorithm to optimize the load impedance of an amplifier for the power-added efficiency (PAE), while meeting a desired level of adjacent-channel power ratio (ACPR) [7]. The load impedance optimization approach is demonstrated using laboratory measurements with a microwave load-pull system. While the use of ACPR in these load-pull measurements provides useful information regarding nonlinearity-induced leakage of the main-band signal into the adjacent channel, the ACPR metric does not provide sufficient information to determine overall spectral mask compliance. Therefore, an improved metric is needed to numerically describe the quality of spectral mask compliance as set forth by the RSEC or other governing document. We define a metric to describe spectral mask compliance and demonstrate its successful use in the optimization. The significance of this paper's contribution is the creation of a metric for spectral mask compliance that is useful in load-impedance optimization, and the demonstration of successful PAE optimization under spectral mask constraints. Our previous work in [7] uses the ACPR, which is the total power in the adjacent band; the ACPR metric is not directly useful as a metric of spectral compliance in the out-of-band domain due to the typical slope of the spectral mask in this region. Rather, the ACPR is a measure of the total power in a defined adjacent band, with no reference to the power-versus-frequency profile in this band. As such, the approach of [7] is somewhat disadvantaged, as regulatory checks with a spectral mask still must be performed following the optimization. With the metric we present in this paper, the optimization can successfully be performed while confirming that the final result of the optimization meets the spectral requirements as outlined by the ITU or other governing body.

This paper involves Pareto optimization, an optimization involving a tradeoff between two objectives that depend on the same variables [8–13]. To our knowledge, this paper is the first demonstration of load-impedance tuning for spectral mask compliance, although initial load-pull tuning for ACPR is demonstrated by Sevic [14, 15], and our previous work demonstrates the Pareto optimization of PAE under ACPR constraint [7]. The work of Wu shows that amplifier-related spectral spreading is caused by third- and fifth-order intermodulation distortion [16]. Several recent papers demonstrate other innovations in intelligent impedance tuning for antenna and amplifier matching applications [17–24].

II. A METRIC FOR SPECTRAL MASK COMPLIANCE

A metric for spectral mask compliance is useful in performing the joint optimization. It is important that this metric clearly demonstrate when the waveform is within the spectral compliance boundaries and when it is outside the boundaries. Optimization requires a numerical metric that can either be maximized, minimized, or propelled toward a target value through the search.

Davidson et al. have proposed a method to perform optimization to spectral mask constraints by the use of linear matrix inequalities, and they also discuss convex optimization as it applies to spectral mask criteria, providing example applications in filter and beamformer design [25]. Parr demonstrates an algorithm to numerically generate short time-duration pulses that meet FCC spectral mask constraints for ultrawideband systems [26]. In Parr's method, eigenvalues of a matrix equation representing transmission describe the percentage of the related eigenvector's power that is inside the spectral mask constraints. Larger eigenvalues indicate a larger percentage of the waveform's power that abides within the spectral mask. The paper gives an example of ultrawideband waveform design to fit an FCC spectral mask between 3.1 GHz and 10 GHz [26]. Sheng demonstrates adjustment of waveform parameters to meet spectral mask requirements based on measurement results [27]. Luo provides a pulse-shaping technique for optimizing a waveform for transmission within a spectral mask [28]. Our metric is different in that it is a measurement-based optimization that involves the amplifier matching network. To our knowledge, the present paper is the first to present a real-time amplifier circuit optimization algorithm based on spectral mask compliance.

The metric S_m we propose for capturing the spectral compliance numerically is defined as follows:

$$S_m = \max(s - m) \tag{1}$$

where s is the power, in dBm, that is output from the radar amplifier and m is the value (also in dBm) of the spectral mask. The values of s and m are compared at all frequencies of interest, and the maximum value of $s - m$ (over all frequencies considered) is used for the optimization. If the output spectrum of the transmitter is compliant with the spectral mask, then $s - m$ is less than or equal to zero. A positive value of S_m indicates that the spectrum is not compliant with the mask. If S_m is zero, then the spectrum is marginally compliant, and if S_m is negative, the spectrum is compliant with "room to spare."

Because linearity and efficiency are conflicting objectives for a power amplifier [29], changing the load impedance to increase the power efficiency is expected to result in a decrease in the linearity, and hence an undesirable increase in S_m. Thus, in a typical Pareto optimization for radar transmission, it is expected that the optimum efficiency under the spectral mask constraints will occur when the spectrum approaches marginal compliance with the spectral mask, at S_m slightly less than zero. To summarize, the two criteria for the Pareto optimization are 1) minimization of the spectral mask metric S_m, and 2) maximization of the PAE. The solution

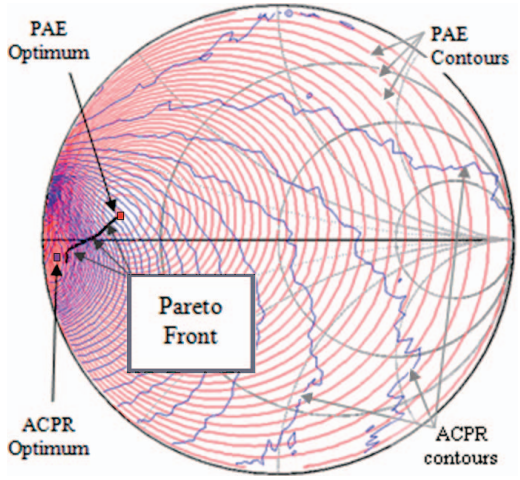

Fig. 1. Typical contour plots for PAE and ACPR. Optimal values of PAE and ACPR are indicated and contours emanate outward from optimum for both. Pareto front is a curve consisting of Pareto optimal solutions between the two optima.

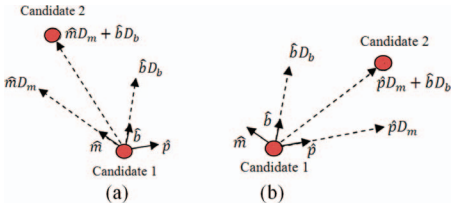

Fig. 2. Graphical description of step vectors in determination of new candidate point for cases (a) when value of S_m is greater than zero (out of compliance with spectral mask) and (b) when value of S_m is less than or equal to zero (in compliance with spectral mask). $\hat{m}$ is unit vector in direction of S_m steepest descent (opposite to S_m gradient), $\hat{p}$ is unit vector in direction of PAE steepest ascent (direction of PAE gradient), and $\hat{b}$ is unit vector in direction of bisector of $\hat{m}$ and $\hat{p}$. Next candidate point is chosen by adding $\hat{m}D_m + \hat{b}D_b$ to current candidate in case (a) and by adding $\hat{p}D_m + \hat{b}D_b$ to current candidate in case (b).

that is chosen from the Pareto front for these two criteria is the solution that results in S_m just below or equal to zero.

III. DESCRIPTION OF THE SEARCH

Fig. 1 shows typical simulated contour plots for the PAE and ACPR. Because the ACPR expresses the power in a defined adjacent channel, the load-impedance dependence of S_m, while not exactly identical, is expected to possess many characteristics similar to the ACPR contours. The concept of Pareto optimization is visible from Fig. 1, as the Pareto optimal solutions lie along a "Pareto front" curve in the Smith chart that contains the optimum PAE values for different limiting values of ACPR. The Pareto front containing the optimum PAE values for different limiting values of S_m is expected to be similar, albeit perhaps distinct. There are two distinct differences (both significant improvements for the optimization) between the optimization for S_m and our previous optimization for ACPR demonstrated in [7].

1) The optimization for S_m is based on the entire spectrum under consideration, not merely total power in a defined adjacent channel. Because the shape of the mask is taken into consideration in the optimization for S_m, the results are expected to be different.

2) While optimization for ACPR using a defined adjacent channel may provide better results in the defined channel but less optimum results in other areas of the spectrum, the S_m optimization will "discover" additional areas of the spectrum that may rise while some channels are decreased. This is important in future joint optimization, where the bandwidth of the input chirp waveform may be varied, causing the third- and fifth-order intermodulation products to appear at different frequencies. In the case of ACPR, this may simply "push" them out of the defined adjacent channel, improving the value of ACPR, but the use of S_m in the optimization will detect these violations of the mask regardless of their frequencies.

The optimization problem at hand is to find the value of load reflection coefficient Γ_L providing the maximum value of PAE while obtaining $S_m \leq 0$. A search is designed that proceeds in a similar manner to the search in [7], using the gradients of PAE and S_m to guide the search. Fig. 2 provides a graphical illustration of choosing the next candidate point during the search. To construct the vector to the next candidate point, the gradients of PAE and S_m are estimated, and unit vectors $\hat{p}$ and $\hat{m}$ are established in the direction of these gradients, respectively. From the theory of convex Pareto optimization, at all points on the Pareto front, $\hat{p}$ and $\hat{m}$ are collinear and oppositely directed [30, 31]. As such, the unit vector $\hat{b}$ bisecting $\hat{p}$ and $\hat{m}$ is directed toward the linear estimate of the closest point on the Pareto front to the present candidate. The vector to the next candidate is composed of a component toward either the PAE or S_m optimum, and a component toward the closest point on the Pareto front (in the direction of $\hat{b}$). Ideally, this will guide the search toward the point with maximum PAE at $S_m = 0$. If measurements of PAE and S_m are performed at the present candidate and $S_m > 0$, the present value of Γ_L does not provide a spectrum in compliance with the spectral mask, and the search vector to find the next candidate point from the present Smith chart location is given by

$$\bar{v} = \hat{m}D_m + \hat{b}D_b \tag{2}$$

where $\hat{m}$ is the unit vector in the direction opposite to the S_m gradient and $\hat{b}$ is the unit vector in the direction of the bisector between $\hat{m}$ and $\hat{p}$, the unit vector in the direction of the PAE gradient. If, however, the measurement gives $S_m \leq 0$, the current candidate Γ_L produces a spectrum that meets compliance requirements, and the vector to the next candidate point from the present Smith chart location is given by

$$\bar{v} = \hat{p}D_m + \hat{b}D_b \tag{3}$$

In this case, the unit vector $\hat{p}$ in the direction of the PAE gradient is used, as it is desired to increase PAE and move

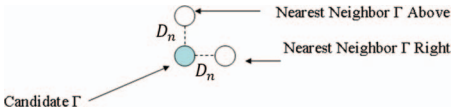

Fig. 3. Measurements to extract gradients for PAE and S_m.

toward the compliance $S_m = 0$ boundary. The vector component magnitudes in (2) and (3) are calculated as follows:

$$D_m = \frac{D_s}{2} \frac{|S_{m,meas}|}{|S_{m,worst}|} \tag{4}$$

$$D_b = \frac{D_s}{2} \frac{|\theta_{meas} - \theta_{target}|}{\theta_{target}} \tag{5}$$

In (4), $S_{m,meas}$ is the value of S_m at the present candidate, and $S_{m,worst}$ is the largest magnitude of S_m over all the measured points since the start of the algorithm. In (5), θ is the angle between $\hat{b}$ and $\hat{m}$, or equivalently, the angle between $\hat{b}$ and $\hat{p}$. θ_{meas} is the measured value of θ at the present candidate, and θ_{target} is the desired value of θ. D_m and D_b are the vector components, and (4) and (5) represent efforts to gauge the remaining distance to the Pareto optimum based on a rough measurement of what percentage of the optimization has been performed regarding each goal. Equation (4) represents an estimate of the percentage of required improvement from the worst case measured value for S_m: the goal value of S_m is zero, and as the candidate approaches the desired value of zero, the step size gets smaller (division by the largest magnitude of S_m measured in the search iterations is performed). Equation (5) gives the component size in the direction of the bisector between the optimum PAE and S_m directions. If the point lies exactly on the Pareto front between the PAE and S_m optima, $\hat{p}$ and $\hat{m}$ will be collinear and oppositely directed, and the value of θ will be 90°. Thus, (5) is an estimate of the "closeness" to the Pareto front, and $\theta_{target} = 90°$ in (5). The value of D_b will decrease as the search nears the Pareto front. The components (4) and (5) thus combine to drive the search toward the desired Pareto optimum by their use in (2) and (3).

To provide the information necessary to choose the next candidate point, the gradients $\nabla p\,(\Gamma_r, \Gamma_i)$ and $\nabla S_m\,(\Gamma_r, \Gamma_i)$ must be calculated. For each candidate value of Γ_L, these are evaluated from measurements at neighboring Γ_L values, separated from the candidate by neighboring point distance D_n, in a manner similar to that described in [24]. The gradient estimation from measurements of PAE and S_m taken at neighboring points is shown conceptually in Fig. 3, based on a method recommended by Wilde [32].

Once the search enters the acceptable region ($S_m \leq 0$), the search is confined to remain in this region by rejecting any measured candidate values of Γ_L that occur with $S_m > 0$. After violation of the mask in this way, the value of search distance parameter D_s in (4) and (5) is divided by 3, and the search is continued. When D_s is found to be less than the distance resolution parameter D_n, the search is stopped, and the measured Γ_L value with the highest value of PAE and $S_m \leq 0$ is selected as the optimum.

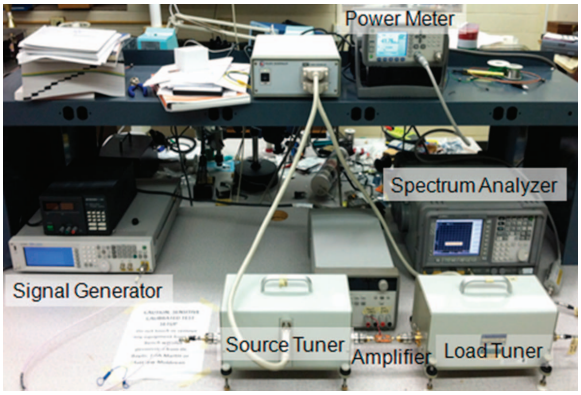

Fig. 4. Load-pull test setup.

IV. MEASUREMENT RESULTS

The algorithm was evaluated using measurements taken using an automated tuner system (ATS) from Maury Microwave controlled by MATLAB. Measurement results were obtained for a Skyworks 65017-70LF InGaP packaged amplifier, with the algorithm starting at different values of Γ_L. The load-pull measurement setup in our laboratory, used for these experiments, is displayed in Fig. 4. The chirp waveform is supplied by a signal generator. The load impedance shown to the device under test is adjusted by a mechanical load tuner. A spectrum analyzer is used to measure the output spectrum, and the measured spectrum is compared by MATLAB to the spectral mask for calculation of S_m. A broadband power sensor and power meter combination is used to measure the broadband output power and calculate the PAE based on the dc power supplied to the device.

As a conceptual point of reference, load-pull contours for PAE and ACPR were measured traditionally for the 65017-70LF amplifier under chirp excitation. The center frequency of the chirp is 3.3 GHz, and the chirp bandwidth of the input waveform is 16 MHz. The contours are shown in Fig. 5. ACPR contours are shown instead of S_m contours because S_m contours are not an option for traditional measurement with the Maury ATS software. However, it is expected that the S_m contours will possess similar characteristics to the ACPR contours, as both metrics are related to adjacent-channel spreading from power amplifier nonlinearities.

For this optimization, the highest PAE value possible while maintaining $S_m \leq 0$ dBc is sought. This provides the best value of PAE while keeping the device within spectral compliance.

Fig. 6 shows the algorithm measurement search results for a starting reflection coefficient $\Gamma_L = 0.9 < 0°$. A PAE of 6.780% is achieved with 11 measurements, and the final value of S_m is slightly less than 0 dBc, as desired. The 11

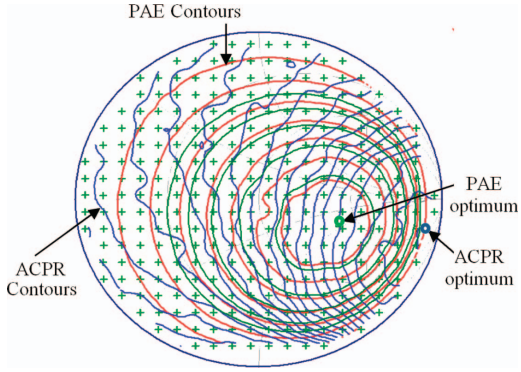

Fig. 5. Traditionally measured PAE and ACPR load-pull contours with PAE and ACPR optima indicated. S_m contours are expected to be similar in shape and trajectory to ACPR contours. For this measurement, main channel is defined from 3.295 GHz to 3.305 GHz, with lower adjacent channel defined from 3.280 GHz to 3.290 GHz.

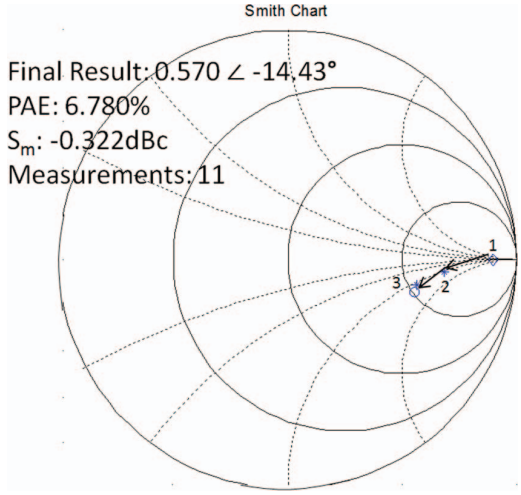

Fig. 6. Measurement search algorithm results from starting $\Gamma_L = 0.9 < 0^\circ$.

measurements required to complete the search is an attractively small number that is comparable to the PAE/ACPR Pareto search detailed in [7].

Figs. 7–10 show additional search algorithm results from different starting values of Γ_L. The results of these searches are summarized in Table I. Table I shows that all of the starting points used in the measurement algorithm resulted in very similar PAE values. The standard deviation of the five PAE values reported is 0.094 percent. This provides significant insight to the reliability of the search to obtain a high value of PAE regardless of starting point. While the endpoints have some variation, most notably from the starting $\Gamma_L = 0.9 < -90^\circ$, the similarity of the PAE values shows that this difference in Smith chart location is inconsequential. This indicates that the PAE does not vary significantly over the region of the endpoints: the characteristic surface over the Smith chart representing the PAE is reasonably flat in the region containing the search endpoints. All five endpoints also show values of S_m less than zero, indicating spectral mask compliance. In addition, all searches end close to the spectral mask, with $S_m > -0.5$ dBc for all endpoints. This

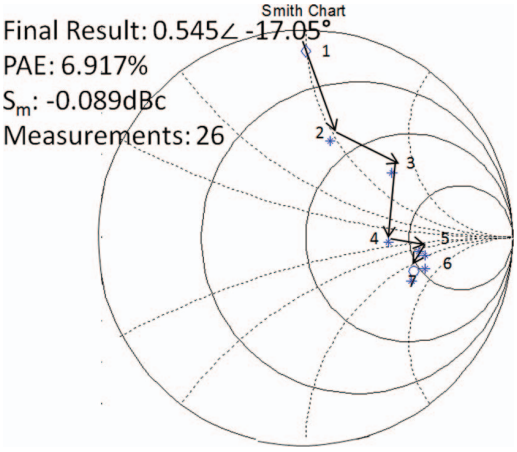

Fig. 7. Measurement search algorithm results from starting $\Gamma_L = 0.9 < 90^\circ$.

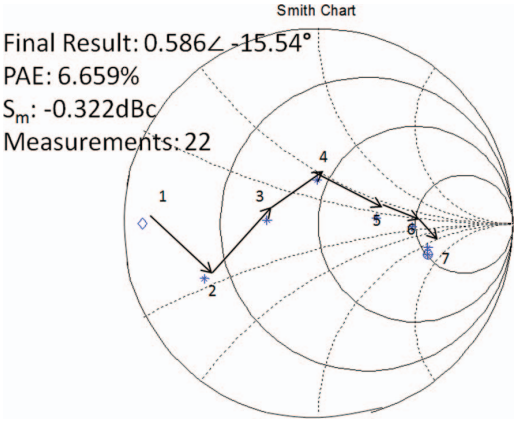

Fig. 8. Measurement search algorithm results from starting $\Gamma_L = 0.9 < 180^\circ$.

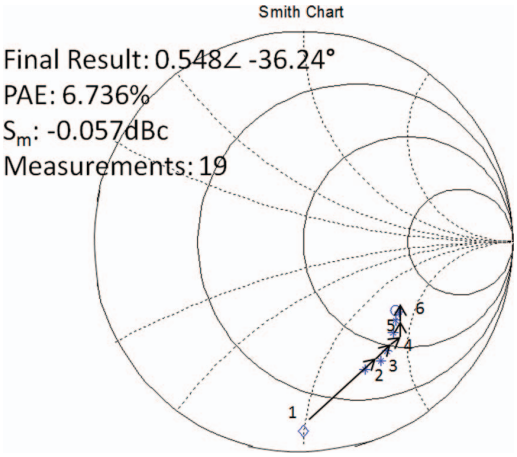

Fig. 9. Measurement search algorithm results from starting $\Gamma_L = 0.9 < -90^\circ$.

indicates that the final Pareto solution of all searches was obtained close to the spectral mask boundary, as expected. The variation of the measurement results in this case appears to be due to measurement noise and the small sensitivity of the PAE characteristic to changes in Γ_L (rather than, for example, to undesirable multimodal PAE and ACPR behavior).

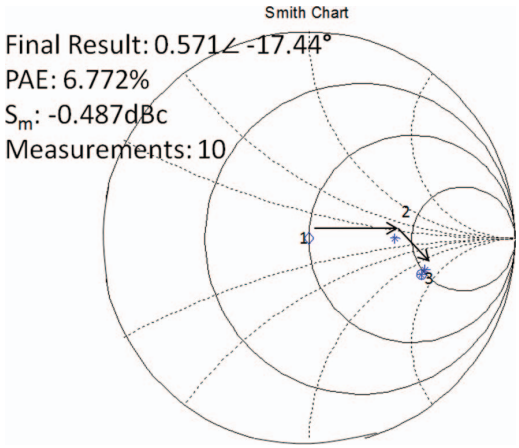

Fig. 10. Measurement search algorithm results from starting $\Gamma_L = 0$.

TABLE I
Measurement Results for Different Starting Reflection Coefficients

Start Γ_L	End Γ_L	End PAE (%)	End S_m (dBc)	# Pts.
$0.9 < 0°$	$0.570 < -14.43°$	6.780	−0.322	11
$0.9 < 90°$	$0.545 < -17.05°$	6.917	−0.089	26
$0.9 < 180°$	$0.586 < -15.54°$	6.659	−0.322	22
$0.9 < -90°$	$0.548 < -36.24°$	6.736	−0.057	19
0	$0.571 < -17.44°$	6.772	−0.487	10

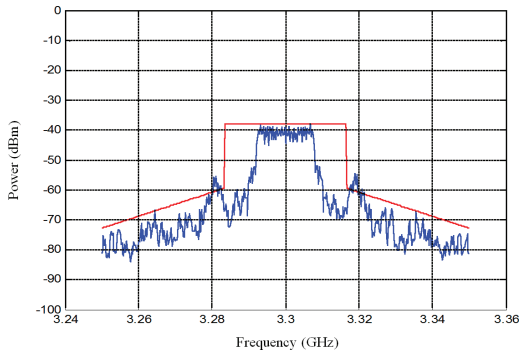

Fig. 11. Spectrum analyzer measurement of signal power versus frequency at starting point $\Gamma_L = 0.9 \angle -90°$ pictured with spectral mask. Spectrum clearly violates spectral mask constraint at multiple points.

Figs. 11 and 12 show the measured power spectrum from the spectrum analyzer for the starting and ending values of Γ_L, respectively, for the search beginning from $\Gamma_L = 0.9 < -90°$, along with the spectral mask used in the optimization. As in the case of typical government-established spectral requirements, the spectral mask is determined from the maximum in-band power of the signal. Fig. 11 shows clear violation of the spectral mask at multiple frequencies above and below the band at the starting value of Γ_L for the search. However, following the optimization, it can be seen that the spectral mask comes just into compliance, with an ending $S_m = -0.057$dBc. This value indicates a very small minimum difference between the spectrum and the mask at the search endpoint, and it appears from Fig. 12 that this minimum difference occurs just below 3.32 GHz, where

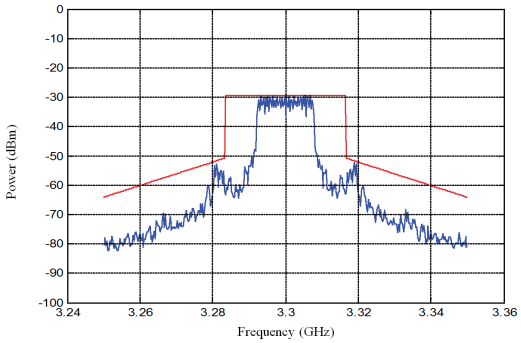

Fig. 12. Spectrum analyzer measurement of signal power versus frequency at $\Gamma_L = 0.548 \angle -36.24°$, the endpoint of search starting from $\Gamma_L = 0.9 \angle -90°$, pictured with spectral mask. Spectrum is compliant, with measured power being less than or equal to spectral mask at all frequencies shown. Final S_m value measured during search was −0.057 dBc, indicating minimum difference between spectrum and mask of only 0.057 dBc, occurring near 3.32 GHz.

the measured spectrum appears to nearly touch the mask. The measurement data shows consistency between spectral mask evaluation and the search results. The search achieves a maximum constrained PAE (constrained to meet spectral requirements) in a very small number of measurements.

V. CONCLUSIONS

An algorithm has been presented to tune the load impedance of a power amplifier to optimize the PAE while achieving spectral mask compliance. Measurement testing has provided excellent results, showing that the optimized PAE under spectral mask compliance conditions varies with a standard deviation of less than 0.1 percent from five different starting values of load reflection coefficient. The number of measurements used to obtain the optimum was seen to vary between 11 and 26 experimental queries, a level of fast optimization expected to be useful for the real-time optimization of radar transmitter power amplifiers.

The results presented in this paper are expected to be useful in the real-time optimization of the load impedance of future radar transmitters. These transmitters can be designed to be spectrally sensitive, optimizing their load impedance to achieve high power efficiency while maintaining spectral compliance. This is expected to be useful in allowing radar transmitters to reconfigure accurately between different frequency bands, and in scenarios where quick frequency adjustment is necessary. In potential future scenarios where spectral masks are varied due to user demand for the spectrum, this algorithm will allow radars to adapt quickly and accurately, maintaining maximized efficiency while meeting the changing spectral requirements.

ACKNOWLEDGMENT

The authors wish to thank Agilent Technologies for cost-free loan of the Advanced Design System software and Modelithics for donation of their model libraries.

REFERENCES

[1] Haykin, S.
Cognitive radar: A way of the future.
IEEE Signal Processing Magazine (Jan. 2006), 30–40.

[2] Guerci, J.
Cognitive Radar: The Knowledge-Aided Fully Adaptive Approach. Boston: Artech House, 2010.

[3] International Telecommunication Union. Unwanted Emissions in the Spurious Emission Domain. Standard ITU-R SM.329.

[4] International Telecommunication Union. Unwanted Emissions in the Out-of-band Domain, Standard ITU-R SM.1541.

[5] International Telecommunication Union. Tables of Maximum Permitted Power Levels for Spurious or Spurious Domain Emissions. Radio Regulations Appendix 3 (Rev. WRC-03).

[6] U.S. National Telecommunications and Information Administration. Radar Spectrum Engineering Criteria, Jan. 2008.

[7] Fellows, M., Baylis, C., Martin, J., Cohen, L., and Marks, R. J., II.
Direct algorithm for the Pareto load-pull optimization of power-added efficiency and adjacent-channel power ratio.
IET Radar, Sonar & Navigation, **8**, 9 (Dec. 2014), 1280–1287.

[8] Calpine, H. C., and Golding, A.
Some properties of Pareto-optimal choices in decision problems.
Omega, **4**, 2 (1976), 141–147.

[9] Getachew, T., Kostreva, M., and Lancaster, L.
A generalization of dynamic programming for Pareto optimization in dynamic networks.
RAIRO-Operations Research, **34**, 1 (2000), 27–47.

[10] Marler, R. T., and Arora, J. S.
Survey of multi-objective optimization methods for engineering.
Structured and Multidisciplinary Optimization, **26**, 6 (2004), 369–395.

[11] Deb, K.
Multi-objective optimization.
In *Search Methodologies*. New York: Springer, 2005, pp. 273–316.

[12] Das, I., and Dennis, J. E.
Normal-boundary intersection: A new method for generating the Pareto surface in nonlinear multicriteria optimization problems.
SIAM Journal on Optimization (Mar. 1998), 631–657.

[13] Kim, I. Y., and de Weck, O.
Adaptive weighted sum method for multiobjective optimization: A new method for Pareto front generation.
Structural and Multidisciplinary Optimization, **31** (2006), 105–116.

[14] Sevic, J., Burger, K., and Steer, M.
A novel envelope-termination load-pull method for ACPR optimization of RF/microwave power amplifiers.
1998 IEEE MTT-S International Microwave Symposium Digest, Vol. 2, June 1998, 723–726.

[15] Sevic, J.
Large signal automated load-pull characterization of adjacent-channel power ratio for digital wireless communication systems.
1996 IEEE MTT-S International Microwave Symposium Digest, June 1996, pp. 763–766.

[16] Wu, Q., Xiao, H., and Li, F.
Linear power amplifier design for CDMA signals: A spectrum analysis approach.
Microwave Journal (1998).

[17] Sun, Y.
Evolutionary tuning method for automatic impedance matching in communication systems.
Proceedings of the 1998 IEEE International Conference on Electronics, Circuits, and Systems, Vol. 3, 1998, pp. 73–77.

[18] Sun, Y., and Lau, W. K.
Antenna impedance matching using genetic algorithms.
Proceedings of the IEE Conference on Antennas and Propagation, York, United Kingdom, Aug. 1999, pp. 31–36.

[19] Qiao, D., Molfino, R., Lardizabal, S., Pillans, B., Asbeck, P., and Jerinic, G.
An intelligently controlled RF power amplifier with a reconfigurable MEMS-varactor tuner.
IEEE Transactions on Microwave Theory and Techniques, **53**, 3, Part 2 (Mar. 2005), 1089–1095.

[20] du Plessis, W., and Abrie, P.
Lumped impedance matching using a hybrid genetic algorithm.
Microwave and Optical Technology Letters, **37**, 3 (May 2003), 201–212.

[21] Arroyo-Huerta, E., Diaz-Mendez, A., Ramirez Cortes, J., and Garcia, J.
An adaptive impedance matching approach based on fuzzy control.
52nd IEEE International Midwest Symposium on Circuits and Systems, Aug. 2009, pp. 889–892.

[22] Hemminger, J.
Antenna impedance matching with neural networks.
International Journal of Neural Systems, **15**, 5 (2005), 357–361.

[23] Mushi, A., Johns, D., and Sedra, A.
Adaptive impedance matching.
Proceedings of the IEEE International Symposium on Circuits and Systems (ISCAS '94), Vol. 2, 1994, pp. 69–72.

[24] Baylis, C., Dunleavy, L., Lardizabal, S., Marks, R. J., II, and Rodriguez, A.
Efficient optimization using experimental queries: A peak-search algorithm for efficient load-pull measurements.
Journal of Advanced Computational Intelligence and Intelligent Informatics, **15**, 1 (Jan. 2011).

[25] Davidson, T. N., Luo, Z.-Q., and Sturm, J. F.
Linear matrix inequality formulation of spectral mask constraints with applications to FIR filter design.
IEEE Transactions on Signal Processing, **50**, 11 (Nov. 2002), 2702–2715.

[26] Parr, B., Cho, B., Wallace, K., and Ding, Z.
A novel ultra-wideband pulse design algorithm.
IEEE Communications Letters, **7**, 5 (May 2003), 219–221.

[27] Sheng, H., Orlik, P., Haimovich, A., Cimini, L., Jr., and Zhang, J.
On the spectral and power requirements for ultra-wideband transmission.
IEEE International Conference on Communications, Vol. 1, May 2003, pp. 738–742.

[28] Luo, X., Yang, L., and Giannakis, G. B.
Designing optimal pulse-shapers for ultra-wideband radios.
2003 IEEE Conference on Ultra Wideband Systems and Technologies, Nov. 2003, pp. 349–353.

[29] Raab, F., Asbeck, P., Cripps, S., Kenington, P, Popovic, Z., Pothecary, N., Sevic, J., and Sokal, N.
Power amplifiers and transmitters for RF and microwave.
IEEE Transactions on Microwave Theory and Techniques, **50**, 3 (Mar. 2002), 814–826.

[30] Martin, J.
Adaptive load impedance optimization for power amplifiers in reconfigurable radar transmitters.
M.S.E.C.E. thesis, Baylor University, 2012.

[31] Lovison, A.
Singular continuation: Generating piecewise linear approximations to Pareto sets via global analysis.
SIAM Journal of Optimization, **21**, 2 (2011), 463–490.

[32] Wilde, D.
Optimum Seeking Methods, Upper Saddle River, NJ: Prentice-Hall, 1964.

Matthew Fellows (S'14) completed the B.S. and M.S. degrees in electrical and computer engineering at Baylor University, Waco, TX in 2012 and 2014, respectively. He is currently pursuing his Ph.D. at Baylor.

His research is focusing on the creation of algorithms for the joint optimization of radar transmitter power amplifier circuitry and waveforms.

Mr. Fellows has published several papers related to his areas of interest.

Charles Baylis (S'03—M'08) received the B.S., M.S., and Ph.D. degrees in electrical engineering from the University of South Florida, Tampa, in 2002, 2004, and 2007, respectively.

He is an Associate Professor of Electrical and Computer Engineering at Baylor University, where he directs the Wireless and Microwave Circuits and Systems (WMCS) Program. His research focuses on spectrum issues in radar and communication systems, and has been sponsored by the National Science Foundation and the Naval Research Laboratory. He has focused his work on the application of microwave circuit technology and measurements, combined with intelligent optimization algorithms, to creating reconfigurable transmitters.

Dr. Baylis serves as the general chair of the annual Texas Symposium on Wireless and Microwave Circuits and Systems, technically co-sponsored by the IEEE Microwave Theory and Techniques Society (MTT-S). He also serves as Student Activities Chair of the IEEE MTT-S Dallas Chapter.

Lawrence Cohen (M'87—SM'12) received a B.S. degree in electrical engineering from The George Washington University, Washington, D.C. in 1975 and an M.S. degree in electrical engineering from Virginia Tech, Blacksburg, VA in 1994.

For the past 26 years he has been employed by the Naval Research Laboratory in Washington, D.C. He has been involved in electromagnetic compatibility (EMC) engineering and management, shipboard antenna integration, and radar system design for 33 years. In this capacity he has worked in the areas of shipboard electromagnetic interference (EMI) problem identification, quantification and resolution, mode-stirred chamber research and radar absorption material (RAM) design, test, and integration. In March of 2007 Mr. Cohen acted as the Navy's Principal Investigator in the assessment of radar emissions on a WiMAX network. Additionally, he has acted as the Principal Investigator for various radar programs, including the radar transmitter upgrades. Currently, he is involved with identifying and solving spectrum conflicts between radar and wireless systems as well as research into spectrally cleaner power amplifier designs, tube and solid state.

Mr. Cohen is certified as an EMC engineer by the National Association of Radio and Telecommunications Engineers (NARTE). He served as the Technical Program Chairman for the IEEE 2000 International Symposium on EMC and was elected for a three-year term to the IEEE EMC Society Board of Directors in 1999 and 2009. He is also a member of the IEEE EMC Society Technical Committee 6 (TC-6) for Spectrum Management.

Robert J. Marks II (F'94), is Distinguished Professor of Engineering in the Department of Engineering at Baylor University.

Dr. Marks is the author of hundreds of journal and conference papers. Some of them are good. His latest book, co-edited with M. Behe, W. Dembski, B. Gordon, and J. C. Sanford, is *Biological Information - New Perspectives* (World Scientific, 2013). He is also the (co)author/(co)editor of *Neural Smithing: Supervised Learning in Feedforward Artificial Neural Networks* (MIT Press)*, Handbook of Fourier Analysis and Its Applications* (Oxford University Press), *Introduction to Shannon Sampling and Interpolation Theory* (Springer-Verlag), *Advanced Topics in Shannon Sampling and Interpolation Theory* (Springer-Verlag), *Fuzzy Logic Technology and Applications* (IEEE Press), *Computational Intelligence: Imitating Life* (IEEE Press), and *Computational Intelligence: A Dynamic System Perspective* (IEEE Press).

He is the recipient of a NASA Tech Brief Award and a best paper award from the American Brachytherapy Society for prostate cancer research. He is Fellow of The Optical Society of America. His consulting activities include Microsoft Corporation, Pacific Gas & Electric, and Boeing Computer Services. His research has been funded by organizations such as the National Science Foundation, General Electric, Southern California Edison, EPRI, the Air Force Office of Scientific Research, the Office of Naval Research, the Whitaker Foundation, Boeing Defense, the National Institutes of Health, The Jet Propulsion Lab, Army Research Office, and NASA.

He was awarded the IEEE Outstanding Branch Councilor Award, The IEEE Centennial Medal, the IEEE Computational Intelligence Society Meritorious Service Award, the IEEE Circuits and Systems Society Golden Jubilee Award, and an IEEE CIS Chapter of the IEEE Dallas Section Volunteer of the Year award. He was named a Distinguished Young Alumnus of Rose-Hulman Institute of Technology, is an inductee into the Texas Tech Electrical Engineering Academy, and in 2007 was awarded the Banned Item of the Year from the Discovery Institute. He was also co-recipient of a NASA Tech Brief Award for the paper "Minimum Power Broadcast Trees for Wireless Networks", and the Judith Stitt Award at the American Brachytherapy Society 23rd Annual Meeting. Dr. Marks served as a Distinguished Lecturer for the IEEE Computational Intelligence Society. He was given IEEE Dallas Chapter Volunteer of the Year Award from the Dallas IEEE CIS Chapter. Dr. Marks served for 17 years as the faculty advisor to the University of Washington's chapter of Campus Crusade for Christ. In 2010, he was listed by CollegeCrunch.com as one of "The 20 Most Brilliant Christian Professors," and, in 2013, one of "the 50 smartest people of faith" at TheBestSchools.org. He has an embarrassingly low Erdős-Bacon number of five.